Properties of the CdSe(0001), (000$\bar{1}$), and (11$\bar{2}$0) Single Crystal Surfaces: Relaxation, Reconstruction, and Adatom and Admolecule Adsorption

Jane Y. Rempel,[†] Bernhardt L. Trout,[†] Moungi G. Bawendi,[‡] and Klavs F. Jensen*[,†]

Department of Chemical Engineering, Massachusetts Institute of Technology, Cambridge, Massachusetts 02139, and Department of Chemistry, Massachusetts Institute of Technology, Cambridge, Massachusetts 02139

Received: June 29, 2005; In Final Form: August 8, 2005

Details of the chemical mechanism underlying the growth of colloidal semiconductor nanocrystals remain poorly understood. To provide insight into the subject, we have preformed a comprehensive study of the polar (0001) and (000$\bar{1}$) and nonpolar (11$\bar{2}$0) wurtzite CdSe surfaces that are exposed during crystal growth using first-principles density functional theory (DFT-GGA) calculations. Stabilization of these surfaces by relaxation and reconstruction was considered. Two particular reconstructions of the polar surfaces were examined: vacancy formation on a 2×2 unit cell and addition of Se and Cd atoms on the (0001) and (000$\bar{1}$) surfaces, respectively. Calculation results indicate that the (11$\bar{2}$0) is the most stable surface when compared to the two polar surfaces. Furthermore, reconstructions of the (0001) surface are energetically favored when compared to reconstructions of the (000$\bar{1}$) facet. Adsorption of Cd and Se atoms and the CdSe molecule on the three relaxed surfaces and two reconstructed (0001) surfaces were also investigated. Several binding sites were considered to determine the most stable binding geometries and energetics. Atomic species preferentially bind in either 2-fold or 3-fold sites, while the CdSe molecule binds parallel to the surface on all of the considered surfaces. Vibrational frequencies of the adspecies were calculated for the most stable binding configurations and were included in the zero point energy correction. Diffusion barriers for the atomic and molecular species were estimated where possible to be between 0.2 and 0.4 eV on the three relaxed surfaces. Thermochemistry of the CdSe molecule binding and dissociation was also investigated. On all considered surfaces, dissociation is preferred to desorption with dissociation only exothermic on the (000$\bar{1}$) surface. Comparison of the three relaxed and two reconstructed surfaces indicates that CdSe molecule binding and dissociation is thermodynamically favored on the (000$\bar{1}$) surface. This implies that under a reaction-controlled regime, the rate of homoepitaxy would be faster on the (000$\bar{1}$) Se terminated surface than on the (0001) and (11$\bar{2}$0) surfaces, making the (000$\bar{1}$) surface of a nanocrystal the primary direction of growth.

Introduction

CdSe is a promising semiconductor material for use in a variety of nanotechnology applications. For example, as a result of their unique size and property relations, CdSe colloidal nanocrystals (quantum dots) have generated tremendous interest in the scientific and industrial communities,[1,2] spanning a broad range of applications from biological labels[3] to electroluminescent devices[4] and lasers.[5] Recent advances in the synthesis of II−VI semiconductor nanocrystals have made it possible to achieve size-selective preparation of high-quality quantum dots either in batch[6,7] or in continuous flow[8] modes. Furthermore, modification of the chemistry has led to synthesis of nanocrystals of more exotic shapes, such as rods and tetrapods.[9,10] However, despite a tremendous effort in developing adaptable chemistries, the underlying mechanisms leading to crystal growth in these systems are still largely unknown, a shortfall which might ultimately limit the versatility, applicability, and mass production of these systems.

Experimental methods to study reactive processes occurring during growth at the surface of a nanocrystal are limited by the inability to isolate elementary reaction steps. As a result, several theoretical studies have been aimed at studying the crystal growth of CdSe. For example, simple models of first-order reaction and diffusion processes have been applied to examine the evolution of an ensemble of nanoparticles.[11] Similarly, a classical model of nucleation and first-order growth was used to fit experimental nanocrystal growth data.[12] However, these models only give qualitative understanding of crystal growth and fail to predict observed results when chemistry is slightly altered or when considering anisotropic growth. Other theoretical studies have been carried out to investigate specifically the nanocrystal surfaces. Simple force field calculations have been applied to study the structures of the trioctylphosphine oxide passivated nanocrystal surfaces.[13] A tight-binding model has also been used to study surface properties of the nonpolar facets of CdSe.[14] A DFT-LDA study was performed by Manna et al., investigating unpassivated and methylamine and methylphosphonic acid passivated surfaces of CdSe.[15] Herein, we explore the fundamental surface reactions that occur during crystal growth, specifically, the homoepitaxy via addition of the Cd and Se atoms and CdSe molecules on the various facets of CdSe.

In particular, we focus on the polar (0001) and (000$\bar{1}$) surfaces and the nonpolar (11$\bar{2}$0) surface of CdSe that have been shown to correspond to the top, bottom, and sides of quantum dots and quantum rods.[16] First, we explore the intrinsic stability of the surfaces and the effect of surface relaxation and compare

* To whom correspondence should be addressed. Address: Department of Chemical Engineering, Room 66-566, 77 Massachusetts Avenue, Cambridge, MA 02139. E-mail: kfjensen@mit.edu. Tel: (617) 253-4589. Fax: (617) 258-8224.
[†] Department of Chemical Engineering.
[‡] Department of Chemistry.

10.1021/jp053560z CCC: $30.25
Published on Web 09/22/2005

our results to previous calculations. Second, we consider several possible reconstructions of the polar surfaces that can alter the growth dynamics. Emphasis is placed on the vacancy and adatom reconstructions that have been prevalent in other II−VI and III−V semiconductors.[17,18] Next, we study the addition of the growth species: Cd and Se atoms and CdSe molecules and map out the stable binding sites and binding energetics on the relaxed and reconstructed surfaces. And last, we compare the binding and dissociation energetics of the CdSe molecule and relate these findings to available experimental observations of anisotropic growth. The computational method of choice for this work is periodic density functional theory (DFT-GGA) that has been extensively applied in the past to study reactive processes occurring on semiconductor surfaces.[19−21]

1. Methods

1.1. DFT Calculations. All of the calculations were performed using DACAPO,[22] a periodic total energy density functional theory code. Cadmium and selenium core electrons were described by ultrasoft pseudopotentials,[23] with the base configuration of Cd ($4d^{10}5s^25p^0$) and Se ($4s^24p^4$) for the 12 cadmium and 6 selenium valence electrons. The Kohn−Sham one-electron valence states were expanded using a basis set of plane waves with a kinetic energy cutoff of 25 Ry. The exchange-correlation energy and potential were described self-consistently with a generalized gradient approximation using a GGA-PW91 functional.[24,25] The density was determined by iterative diagonalization of the Kohn−Sham Hamiltonian, Fermi population of the Kohn−Sham states ($k_BT = 0.1$ eV), and Pulay mixing of the resulting electronic density.[26] All total energies were extrapolated to $k_BT = 0$ eV. To speed up the calculations, a $2 \times 2 \times 1$ Monkhorst−Pack[27] k-point set was used in all the surface energy and surface adsorption calculations. Convergence of the total energy and binding energies was checked by increasing the k-point set to $4 \times 4 \times 1$ and to $8 \times 8 \times 1$ and increasing the cutoff energy to 35 Ry. The values were converged to 0.1 and 0.01 eV for the total energy and binding energies, respectively. To verify the accuracy of the pseudopotentials, bulk lattice parameters were calculated for the wurtzite and zinc blende structures of CdSe. The calculated wurtzite lattice parameter of 4.38 Å is within 1.9%[28] of the experimental value and zinc blende lattice parameter of 6.19 Å is within 2.3%.[28] All the bulk calculations were performed using $8 \times 8 \times 8$ Monkhorst−Pack[27] k-point set with the convergence rigorously verified by varying the k-point set between $2 \times 2 \times 2$ and $10 \times 10 \times 10$ and increasing the plane wave energy cutoff to 40 Ry.

1.2. Description of the Surfaces. All surfaces were described using a slab model containing four CdSe bilayers as defined in Figure 1. The two polar facets were described by a 2×2 lateral supercell with four Cd and four Se atoms per bilayer (single unit cells of the (0001) and (000$\bar{1}$) surfaces are highlighted in Figure 1). The exposed surfaces contained either four Cd, (0001) surface, or four Se atoms, (000$\bar{1}$) surface, bound to three atoms of the opposite type in the second topmost layer. This supercell geometry is equivalent to a 0.25 ML surface coverage which minimizes the interaction of the neighboring adsorbates. Due to the symmetry of the (11$\bar{2}$0) surface, the smallest possible unit cell contained four Cd and four Se atoms per bilayer, with two Cd and two Se atoms in the topmost layer. In all cases, the top two bilayers were allowed to relax while the bottom two bilayers were fixed in the bulk truncated geometry with a lattice parameter of 4.38 Å. A vacuum of approximately 12 Å was placed above the slabs. Adsorption was only allowed on one of the two exposed surfaces. Furthermore, the electrostatic potential was adjusted[29] in order to decouple dipole interaction of the neighboring slabs: either an intrinsic dipole associated with the (0001) or (000$\bar{1}$) surface models or a dipole generated as a result of adspecies adsorption on the (11$\bar{2}$0) surface.

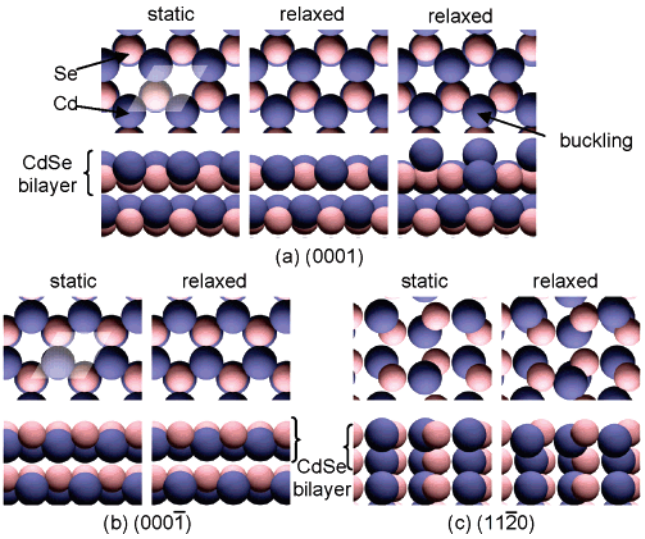

Figure 1. Top and side view of the polar (0001) and (000$\bar{1}$) surfaces and of the nonpolar (11$\bar{2}$0) surface of CdSe. All three surfaces are shown with and without the relaxation of the top two Cd (large spheres) and top two Se (small spheres) layers. In the case of (0001), surface contraction relaxation and surface buckling relaxation are shown.

1.3. Thermodynamic Considerations. 1.3.1. Surface Energies. Surface energies were determined using two different methods. The first was the slab method in which the surface energy is obtained by

$$\sigma_{top} + \sigma_{bottom} = (E_{slab} - n_{CdSe}E_{bulk})/A \quad (1)$$

where E_{slab} is the total energy of the slab, n_{CdSe} is the number of CdSe units in the slab, and A is the area of the supercell. Furthermore, if we introduce surface relaxation, the energy of the relaxed surface can be obtained by

$$\sigma_{top,relaxed} = (E_{slab,relaxed} - n_{CdSe}E_{bulk})/A - \sigma_{bottom} \quad (2)$$

where $E_{slab,relaxed}$ is the total energy of the slab with the top two bilayers relaxed. The second method relies on calculating the surface energy from a series of different size slabs. For this method, we rearrange eq 1

$$E_{slab}/n_{CdSe} = E_{bulk} + A(\sigma_{top} + \sigma_{bottom})/n_{CdSe} \quad (3)$$

and plot the left-hand side as a function of $1/n_{CdSe}$ and calculate a value of the sum of the surface energies from the slope. The value obtained by the slab method (three to six bilayers thick) for the sum of the top and bottom surface energies of the bulk truncated (0001) surface was compared to the value obtained from the slope method and was shown to be within 3 eV/Å^2 or approximately 3%. Unless stated otherwise, the surface energies presented in the paper always refer to the values obtained with the simpler slab method for a slab thickness of four bilayers.

The individual surface energies of the top and bottom surfaces can be easily computed for the (11$\bar{2}$0) surface, which has identical termination on the two sides of the slab ($\sigma_{top} = \sigma_{bottom}$). On the other hand, due to the lack of inversion symmetry in the wurtzite crystal structure, the (0001) and (000$\bar{1}$) surfaces cannot be isolated independently using a slab geometry. A

similar problem arises for the polar (111) and ($\bar{1}\bar{1}1$) surfaces of the zinc blende structure. For this crystal structure, a method of direct calculation of the surface energies was developed by Zhang and Wei[30] and later applied to CdSe.[15] Instead of the slab geometry, they constructed an infinite wedge with a triangular cross section with sides corresponding to the (001), (111), and ($\bar{1}\bar{1}1$) surfaces, where the last two are equivalent to each other. They then compared two successive size wedges to determine the surface energy of the (111) surface. The main shortcoming of this approach is that the total energies of different size wedges are compared and, as a result, the calculated surface energy greatly depends on the total energy convergence. We propose a modification based on energy differences of two structures of the same size, thus relying only on convergence of the energy differences.

If we consider a wedge shaped structure, as described by Zhang and Wei[30] with two equivalent sides made up of n unit cells of Se terminated ($\bar{1}\bar{1}1$) and ($1\bar{1}\bar{1}$) facets and the bottom made up of $n - 1/2$ unit cells of the Cd terminated (001) facet, then the total energy of the wedge is

$$E_{\text{wedge},1} = \frac{n(n+1)}{2} E_{\text{bulk}} + 2nA_{(111)}\sigma_{(\bar{1}\bar{1}1)} + (n - 1/2)A_{(001)}\sigma_{(001),\text{Cd}} + \sum E_{\text{edges},1} \quad (4)$$

where $A_{(111)} = a^2(3)^{1/2}/4$, $A_{(001)} = a^2/2$, and a is the lattice constant of the zinc blende structure. Now, instead of considering a larger size structure, we use the same size structure but interchange the position of the Cd and Se atoms; thus, we rely only on the convergence of the energy differences, which is achieved much faster than the total energy convergence. This second wedge structure contains two equivalent Cd terminated (111) and ($\bar{1}\bar{1}1$) sides and a Se terminated (001) bottom, with the total energy of the wedge

$$E_{\text{wedge},2} = \frac{n(n+1)}{2} E_{\text{bulk}} + 2nA_{(111)}\sigma_{(111)} + (n - 1/2)A_{(001)}\sigma_{(001),\text{Se}} + \sum E_{\text{edges},2} \quad (5)$$

Assuming that the surface energies and the edge energies are not a function of size and plotting the difference, $E_{\text{wedge},1} - E_{\text{wedge},2}$, as a function of n for several different sizes of wedge geometries, we obtain

$$\text{slope} = 2A_{(111)}(\sigma_{(\bar{1}\bar{1}1)} - \sigma_{(111)}) + A_{(001)}(\sigma_{(001),\text{Cd}} - \sigma_{(001),\text{Se}}) \quad (6)$$

If we know the difference of the (001) surface energies and since the sum, $\sigma_{(\bar{1}\bar{1}1)} + \sigma_{(111)}$, can be calculated using a slab method on the zinc blende structure, then we can calculate the surface energies of the polar surfaces independently. Furthermore, since at the surface the nearest neighbor and the next nearest neighbor geometry of the zinc blende and the wurtzite structures are equivalent, the two should have comparable surface energies and, as a result, we can utilize the surface energy difference that we calculated for the zinc blende structure using our modified method to determine the surface energies of the (0001) and ($000\bar{1}$) surfaces. To verify this assumption, we compared the sums of the surface energies for the polar facets of the zinc blende and wurtzite structures computed using a slab geometry of equal sizes were within 1.2% of each other.

A problem arises when we try to calculate surface energies of the (001)Cd and (001)Se surfaces, since the slab geometry for these structures contains an unequal ratio of the Cd and Se atoms and, therefore, eq 1 does not apply. In this case we can use a more general approach, described in detail by Kresse et al.[18] and also applied by Manna et al.[15]

$$\sigma_{\text{top}} + \sigma_{\text{bottom}} = (E_{\text{slab}} - n_{\text{Se}}\mu_{\text{Se}} - n_{\text{Cd}}\mu_{\text{Cd}})/A \quad (7)$$

where μ_{Se} and μ_{Cd} are chemical potentials of the two particle reservoirs. If we assume that the particle reservoirs are in thermal equilibrium with the bulk CdSe, that is, there is no growth or decomposition, then

$$\mu_{\text{Cd}} + \mu_{\text{Se}} = E_{\text{bulk}} \quad (8)$$

Substituting eq 8 into eq 7

$$\sigma_{\text{top}} + \sigma_{\text{bottom}} = (E_{\text{slab}} - n_{\text{Se}}E_{\text{bulk}} + (n_{\text{Se}} - n_{\text{Cd}})\mu_{\text{Cd}})/A \quad (9)$$

For a slab with an equal ratio of Cd and Se atoms, we recover back eq 1. We can place further limits on the chemical potentials

$$\mu_{\text{Cd}} < E_{\text{bulk,Cd}} \quad (10)$$

$$\mu_{\text{Se}} < E_{\text{bulk,Se}} \quad (11)$$

If either inequality is not satisfied, then either Se or Cd would flow to the respective particle reservoirs leaving behind bulk Cd or bulk Se, respectively. Furthermore, if we define the enthalpy of formation as

$$\Delta H_{\text{f,CdSe}} = E_{\text{bulk}} - E_{\text{bulk,Cd}} - E_{\text{bulk,Se}} \quad (12)$$

we can determine the limits for the chemical potential of Cd to be used in eq 9

$$E_{\text{bulk,Cd}} + \Delta H_{\text{f,CdSe}} < \mu_{\text{Cd}} < E_{\text{bulk,Cd}} \quad (13)$$

The lower limit corresponds to Cd poor and the upper limit to the Cd rich conditions. We calculated the heat of formation to be -1.43 eV, which is in close agreement with the DFT-LDA results.[15] Using this scheme, we calculated the limit values of the surface energies of the (001)Se and (001)Cd surfaces and hence the limit surface energies of the polar facets.

1.3.2. Relaxation and Reconstruction Energies. The energy of relaxation was defined as

$$\Delta E_{\text{rel}} = E_{\text{slab,relaxed}} - E_{\text{slab}} \quad (14)$$

Note that for the reconstruction containing an adatom, the energy of the slab is calculated for the surface atoms in the bulk truncated positions and the adatom relaxed to the most stable configuration.

Gas-phase energies of the Cd and Se atoms were used as reference states in calculating the energies of reconstruction, such that the energy of vacancy reconstruction was defined as

$$\Delta E_{\text{rec}} = E_{\text{slab,reconstructed}} - E_{\text{slab,relaxed}} + E_{\text{Cd or Se gas phase}} \quad (15)$$

Similarly, the energy of adatom reconstructions was defined as

$$\Delta E_{\text{rec}} = E_{\text{slab,reconstructed}} - E_{\text{slab,relaxed}} - E_{\text{Cd or Se gas phase}} \quad (16)$$

1.3.3. Binding Energies. Similar to calculating the energy of reconstruction, gas-phase energies of the Cd and Se atoms and the CdSe molecule were chosen as reference states in calculating the binding energy. In general, the binding energy for any adsorbate (A) was defined as

$$\text{BE} = E_{\text{slab+A}} - E_{\text{slab,relaxed}} - E_{\text{A,gas}} \quad (17)$$

TABLE 1: Surface Properties of the Various CdSe Surfaces

	(0001)		(000$\bar{1}$)		(11$\bar{2}$0)
	Cd poor	Cd rich	Cd poor	Cd rich	
σ_{st} (meV/Å^2)	66.1	44.6	34.0	55.5	32.0
σ_{rel} (meV/Å^2)	55.8[a]	34.3[a]	30.9	52.4	15.4
	49.7[b]	28.2[b]			
ΔE_{rel} (eV)	−0.68[a]		−0.20		−0.90
	−1.09[b]				
$\Delta E_{rec,V}$ (eV)	0.33		2.50		
$\Delta E_{rel,V}$ (eV)	−1.73		−1.17		
$\Delta E_{rec,A}$ (eV)	−3.59		−2.09		
$\Delta E_{rel,A}$ (eV)	−1.15		−0.34		

[a] Compression relaxation. [b]Buckling relaxation.

Where E_{slab+A} is the energy of the slab and the adsorbate and $E_{A,gas}$ is the energy of the adsorbate in the gas phase.

Frequencies of the adsorbate normal modes of vibration were determined from eigenvalues of the mass-weighted Hessian matrix, which was obtained using a second-order finite difference method of calculating force derivates. Aside from a few exceptions, the slab atoms were fixed in their relaxed positions and the adsorbate atom(s) was (were) displaced by 0.01 Å in all directions. Increasing the displacement to 0.04 Å did not significantly alter the vibrational frequencies. The binding energies were then corrected by the zero-point energies (ZPE)

$$ZPE_c = ZPE_{slab+A} - ZPE_{A,gas} - ZPE_{slab} \qquad (18)$$

ZPE_{slab} was calculated only for surfaces with one of the surface atoms protruding out of the surface plane, such that the protruding atom was moved, while the remaining slab atoms were fixed in their relaxed positions.

2. Results and Discussion

2.1. CdSe Surfaces: Relaxation. Images of the top and side views of the three static bulk terminated and relaxed (0001), (000$\bar{1}$), and (11$\bar{2}$0) surfaces are shown in Figure 1. The polar (0001) and (000$\bar{1}$) facets consist of a 2 × 2 supercell with one of the unit cells highlighted for reference. The nonpolar (11$\bar{2}$0) surface consists of a single irreducible unit cell with an equal number of atoms as in the 2 × 2 polar supercells. In the relaxed geometries, atoms in the top two bilayers, as defined in Figure 1, are allowed to move until the total energy is minimized. Surface energies of both static and relaxed surfaces and the energy gain due to relaxation for the three surfaces are presented in Table 1.

Relaxation of the polar (0001) and (000$\bar{1}$) facets leads to contraction of the top bilayer, with the effect significantly more pronounced on the Cd terminated (0001) surface with a spacing change of 0.5 vs 0.1 Å on the (000$\bar{1}$) surface. Such a relaxation corresponds to a shift in the orbital hybridization from sp^3 to sp^2 of the topmost atomic layer. Not surprisingly, the energy decrease due to relaxation, as defined in eq 14, is higher for the (0001) surface than that for the (000$\bar{1}$) surface, −0.68 and −0.20 eV per 2 × 2 supercell, respectively (Table 1). We also observe further relaxation of the (0001) facet by buckling, expulsion of one of every four surface Cd atoms (Figure 1a). Buckling leads to an energy decrease of −0.41 eV (Table 1) relative to the contracted surface and a decrease in the dipole moment of the slab from 1.25 to 0.82 eÅ, which is not achieved via surface compression. Furthermore, relaxation of the surface atoms is observed, such that the atoms in the top CdSe bilayer become coplanar, with neighboring Se atoms shifting toward the buckling site. Note that if we had chosen a 1 × 1 unit cell to model the surface, it would have been impossible to observe buckling. Buckling relaxation is not stable on the (000$\bar{1}$) surface, where the protruding atom relaxes back to the contracted geometry. Manna et al. have attributed buckling of the (0001) surface to adsorbate binding;[15] however, we find that buckling is a stable relaxation pathway even in the absence of adsorbates.

Images of the nonpolar (11$\bar{2}$0) surface are presented in Figure 1c. Comparison of the static and relaxed structures shows that relaxation leads to tilting of the CdSe bond relative to the horizontal, with Se coming out of the surface plane. This relaxation is consistent with a transfer of half of an electron from each Cd to each Se, with the shift in Cd orbital hybridization from sp^3 to sp^2, making the local geometry around each surface Cd atom almost planar. The relaxation of the (11$\bar{2}$0) surface leads to an energy decrease of 0.90 eV (Table 1) and a small dipole moment change from 0 to −0.12 eÅ per unit cell. Similar relaxation has been previously shown using tight-binding calculations on the (11$\bar{2}$0) CdSe and CdS surfaces[14] and DFT-LDA calculations on CdSe.[15]

As described earlier, the sums of the top and bottom surface energies of a slab are calculated using either the slab or the slope method, while the difference of the two for the polar facets is obtained using the modified infinite wedge method (see section 1.3.1). The surface energies obtained for the polar facets are given in Table 1 at the two limiting values of the Cd chemical potential, corresponding to a Cd poor and Cd rich case. Note that the surface energy of the nonpolar (11$\bar{2}$0) surface is independent of the Cd chemical potential, and as a result, only a single value is presented in Table 1. Comparison of the surface energies shows that (11$\bar{2}$0) is the most thermodynamically stable surface in the relevant window of Cd chemical potentials, and as a result, we would expect this surface to be less reactive under growth conditions. On the other hand, the (000$\bar{1}$) surface is more stable under Cd poor and the (0001) under Cd rich conditions. This finding is consistent with the fact that the (000$\bar{1}$) surface is Se terminated and the (0001) surface is Cd terminated; hence, under Cd poor conditions, a Se rich surface would be more stable. Note that without a priori knowledge of the Cd chemical potential, the relative stability of the two polar surfaces cannot be determined. The values we obtain for surface energies are lower than those obtained using DFT-LDA calculations.[15] This can be attributed to the difference in computational methods, for example, LDA vs GGA, and the difference in the backside termination methods, pseudo-hydrogen termination vs electrostatic potential correction.

2.2. CdSe Surfaces: Reconstruction. In general, the bulk truncated polar surfaces contain 0.5 e^- per unpassivated Cd bond and 1.5 e^- per unpassivated Se bond on the (0001) and (000$\bar{1}$) surfaces, respectively. Reconstruction of these surfaces either by vacancy formation or by adatom addition allows for the relaxation of the partially filled unpassivated bonds to become either empty or filled. Note that care must be taken in selection of the supercell to make surface reconstructions possible; in particular, the supercell must be selected such that the total number of electrons in the unpassivated surface bonds must be an even number. As a result, we chose a 2 × 2 supercell for the (0001) and (000$\bar{1}$) surfaces that would each contain six or two surface electrons in the case of vacancy and adatom reconstructions, respectively.

Reconstruction via vacancy formation, removing one Cd atom from a 2 × 2 (0001) surface supercell, allows for half an electron transfer from each of the three surface Cd atoms to the three subsurface Se atoms coordinating the vacancy site, leading to a shift in the Cd orbital hybridization from sp^3 to sp^2, with an empty p orbital, and 2 e^- per unpassivated subsurface Se sp^3

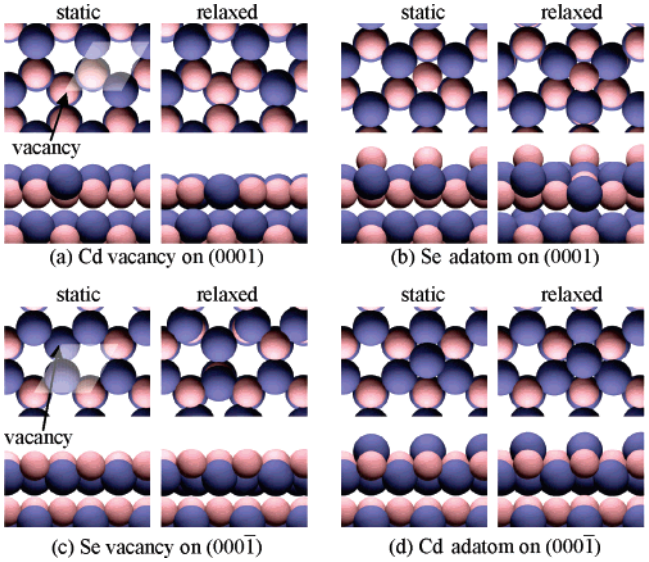

Figure 2. Surface reconstructions of the 2 × 2 supercell of the polar (0001) and (000$\bar{1}$) CdSe surfaces: one vacancy or one adatom per unit cell. Highlighted is a quadrant of the 2 × 2 unit cell.

orbital. Comparison of the static and the relaxed vacancy structures (Figure 2a) shows planarization around surface Cd atoms and an inward shift in the subsurface Se atoms toward the vacancy site, which is consistent with the electron-transfer model. Alternatively, addition of a Se atom to the (0001) surface, would allow for half an electron transfer from the noncoordinating Cd atom to the adsorbed Se, leaving behind an empty p orbital on the Cd atom and a filled sp^3 orbital on the Se adatom. Again, comparing the static and the relaxed structures (Figure 2b) we observe planarization around the noncoordinating surface Cd atom which is also consistent with the shift in orbital hybridization.

Applying the same analysis for vacancy and adatom reconstructions of the Se terminated (000$\bar{1}$) surface, we would expect half of an electron transfer from each of the unpassivated orbitals of the three subsurface Cd atoms to the three surface Se atoms for the vacancy reconstruction and half an electron transfer from the Cd adatom to the noncoordinating surface Se atom for the adatom reconstruction. Comparing surface structures of the vacancy reconstruction of the (000$\bar{1}$) surface (Figure 2c), we observe an outward shift of the subsurface Cd atoms away from the vacancy site, leading to an approximately planarized coordination, which is again consistent with the electron-transfer hypothesis. On the other hand, the Cd adatom (Figure 2d) binds very close to the surface but does not achieve a fully planar geometry; hence, it is difficult to access the extent of electron transfer.

The energies of vacancy and adatom reconstructions of the (0001) and (000$\bar{1}$) surfaces (eqs 15 and 16) and energies of relaxation of these reconstructed surfaces (eq 14) are presented in Table 1. Comparing the energies of relaxation, we see that a significant decrease in energy is obtained as a result of relaxation of the vacancy reconstructions. On the other hand, relaxation of an adatom reconstruction shows a significant energy decrease only on the (0001) surface, which is consistent with the observation that planarization around the Cd adatom is not achieved on the (000$\bar{1}$) surface. The energies of reconstruction (Table 1) show that, in general, vacancy formation, removing one of four surface atoms into vacuum, is an endothermic process. However, the energy cost of vacancy formation is much lower on the (0001) surface than that on the (000$\bar{1}$) surface, 0.33 vs 2.50 eV, and as a result, we would expect vacancy formation to be more likely to occur on the former of the two. Similarly, addition of an adatom from a vacuum is an exothermic process that is more preferable on the (0001) surface, with an energy gain of −3.59 and −2.09 eV on the (0001) and (000$\bar{1}$) surfaces, respectively (Table 1). Note that in calculating the energy of reconstruction, we use atoms in a vacuum as a consistent reference state, such that in an actual system atoms would be further stabilized, decreasing the energy cost of vacancy formation and energy gain of adatom addition. As a result, in all adsorption calculations we choose to include only the most stable (0001) surface vacancy and adatom reconstructions.

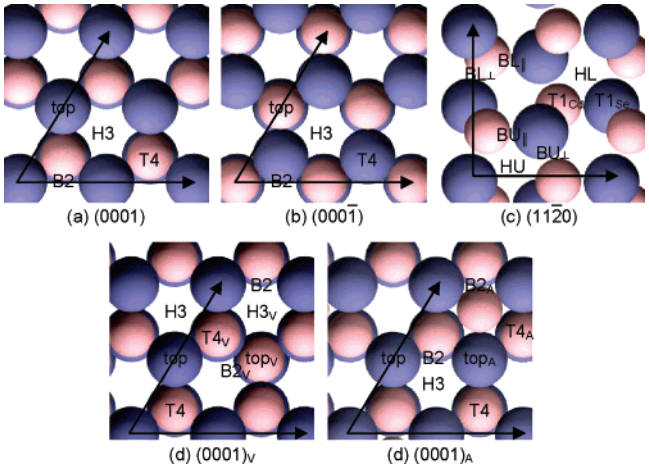

Figure 3. Top view of the three relaxed and two reconstructed CdSe surfaces with the high-symmetry sites labeled.

TABLE 2: Binding Energy of Cd and Se Atoms and the CdSe Molecule on Various Sites of the Fully Relaxed Polar (0001) and (000$\bar{1}$) Surfaces of CdSe[a]

BE (eV)	(0001)			(000$\bar{1}$)		
site	Se	Cd	CdSe	Se	Cd	CdSe
top	−2.64	−0.35		−2.48	−0.95	−2.46
B2	−3.43	−0.13		−2.90	→H3	
H3	−3.59	unstable	−2.78	−2.38	−2.08	−2.54
T4	−3.47	−0.27		−2.57	−1.88	−2.48
[H3−T4]			−2.95			→[H3−B2]
[T4−H3]			−3.19			→[T4−B2]
[H3−B2]			−3.25			−2.63
[T4−B2]			−3.27			−2.58
E_d	0.17		0.32	0.41		0.16

[a] Site labels correspond to parts a and b of Figure 3.

2.3. Adsorption on Polar (0001) and (000$\bar{1}$) Surfaces. Schematic representations of the polar (0001) and (000$\bar{1}$) surfaces with the high-symmetry binding sites labeled are given in parts a and b of Figure 3. To make the notation clear, the top is a 1-fold atop site, B2 is a 2-fold bridge site, H3 is a hollow 3-fold site, and T4 is a tetrahedral 4-fold site. Binding energies of the Cd and Se adatoms and the CdSe molecule at the various sites, as defined in eq 17, are presented in Table 2 with the schematics of the most stable binding configurations shown in Figure 4. For the molecular CdSe adsorbate with dual coordination, the sites for both Cd and Se atoms are listed with Cd atom coordination first. The estimated diffusion barriers are also presented in Table 2.

The Se atom binds very strongly on both the (0001) facet and the (000$\bar{1}$) facet. The H3 (−3.59 eV) and the B2 (−2.90 eV) are the preferred binding sites on the two surfaces, respectively. These binding configurations are consistent with the electron-transfer surface stabilization model, such that, on the (0001) surface, half an electron is transferred from the

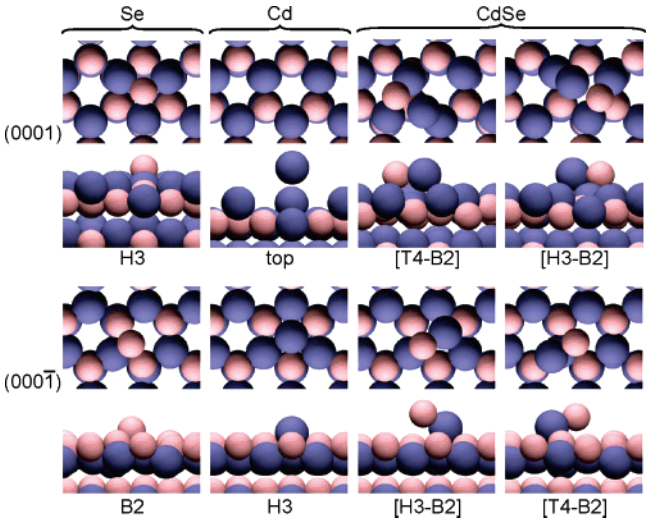

Figure 4. Most stable binding configurations of the Cd and Se atoms and the CdSe molecule on the two polar (0001) and (000$\bar{1}$) surfaces. For simplicity, periodic copies of the adsorbate species are not shown in the images.

noncoordinating Cd to the bound Se atom, and on the (000$\bar{1}$) surface, half an electron is transferred from each of the two coordinating Se atoms to the two noncoordinating ones, thus leading to either empty or filled surface states. The estimated lower bounds on the Se diffusion barrier are 0.17 eV through the B2 site on the (0001) surface and 0.41 eV through the top site on the (000$\bar{1}$) surface (Table 2). It is not surprising that the diffusion barrier is lower on the (0001) surface, since the corresponding intermediate B2 state does not contain any partially occupied electronic states, while the top site coordination on the (000$\bar{1}$) surface does.

The Cd atom is only weakly bound on the Cd terminated (0001) surface but is strongly bound on the (000$\bar{1}$) surface, with the top (−0.35 eV) and H3 (−2.08 eV) being the preferred binding sites. On the buckling (0001) surface, half an electron is transferred from the three surface Cd atoms to the buckling one. Thus, we would expect the surface to be electron deficient with the buckling atom being the most electron donating, and hence, it is not surprising to find the top site is the most stable binding site for Cd. Similarly, on the Se terminated (000$\bar{1}$) surface, binding in a 3-fold site allows for half an electron being transferred from the Cd to the noncoordinating Se atom, thus stabilizing the bound geometry. Since the B2 site on (0001) can be near either a surface or a buckling atom and the B2 site on (000$\bar{1}$) is unstable, it is impossible to estimate the Cd diffusion barrier on either of the polar surfaces.

There are several effectively degenerate binding sites for the CdSe molecule on the two polar surfaces, in particular, the T4−B2 (−3.27 eV) and H3−B2 (−3.25 eV) sites on the (0001) surface and H3−B2 (−2.63 eV) and T4−B2 (−2.58 eV) sites on the (000$\bar{1}$) surface. On the (0001) surface, the adsorbed molecule is parallel to the surface coordinating through both Cd and Se atoms, while on the (000$\bar{1}$) surface, the CdSe molecule binds at an angle to the surface (61° and 71° from the vertical for the two configurations). The latter leads to only weak coordination through the Se atom, and consequently, it is not surprising to find that the CdSe molecule binds more strongly to the (0001) surface. Furthermore, the estimated lower bound for the diffusion barrier is lower on the (000$\bar{1}$) surface, with diffusion occurring through the H3−T4 site (0.32 eV) and through the top site (0.16 eV) on the (0001) and (000$\bar{1}$) surfaces, respectively. Following the same reasoning for the electron transfer, we see that on all surfaces the initial binding configurations allow for electron transfer to eliminate partially filled states, while only the intermediate state for diffusion on the (000$\bar{1}$) surface does, which explains the lower diffusion barrier.

TABLE 3: Binding Energy of the Cd and Se Atoms and the CdSe Molecule on Various Sites of the Fully Relaxed Nonpolar CdSe(11$\bar{2}$0) Surface[a]

BE (eV) site	(11$\bar{2}$0) Se	Cd	CdSe	BE (eV) site
$T1_{Se}$		−0.07	−2.39	$[BL_{\perp}-T1_{Cd}]$
$T1_{Cd}$	$\rightarrow BL_{\parallel}$		−1.85	$[BL_{\parallel}-BU_{\parallel}]$
HL	−2.03	−0.25	−2.59	$[T1_{Se}-T1_{Cd}]_{\parallel}$
$BL_{\parallel}$	−2.07	−0.27	$\rightarrow[T1_{Se}-T1_{Cd}]_{\perp}$	$[T1_{Se}-BL_{\parallel}]$
$BL_{\perp}$	−1.90	−0.30	−2.66	$[T1_{Se}-T1_{Cd}]_{\perp}$
$BU_{\parallel}$	−2.05	−0.14		
$BU_{\perp}$	−2.05	−0.10		
HU	−2.03	−0.25		
$E_d\langle 0001\rangle$	0.04	0.06		
$E_d\langle 10\bar{1}0\rangle$	0.17	0.21		

[a] Site labels correspond to Figure 3c.

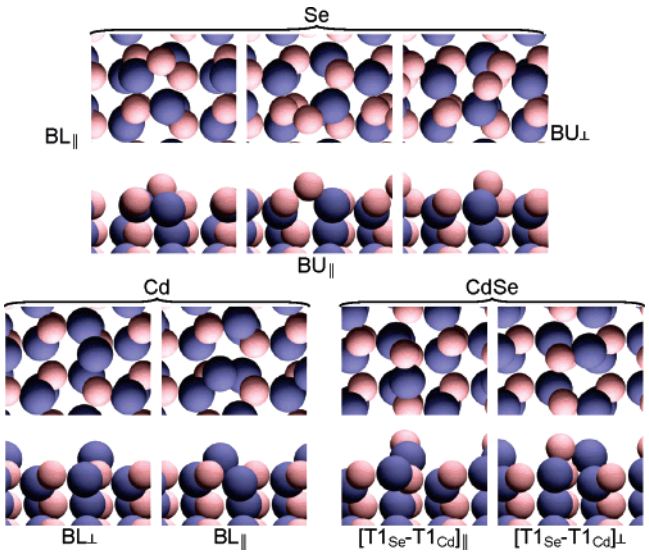

Figure 5. Most stable binding configurations of the Cd and Se atoms and the CdSe molecule on the nonpolar (11$\bar{2}$0) surface.

2.4. Adsorption on the Nonpolar (11$\bar{2}$0) Surface. A schematic of the high-symmetry sites on the nonpolar (11$\bar{2}$0) surface is presented in Figure 3c, with the notation as follows: T1 is a tetrahedral 1-fold site with coordination to either surface Cd or Se, BL and BU are a 2-fold bridge sites above either the lower (L) or upper (U) surface layers running either parallel or perpendicular to the surface CdSe chains, and HL and HU are hollow 4-fold sites. Binding energies of the Cd and Se adatoms and the CdSe molecule at the various sites of the (11$\bar{2}$0) surface are presented in Table 3, with the schematics of the most stable binding configurations shown in Figure 5. The estimated diffusion barriers are also presented in Table 3.

There are a multitude of almost degenerate (−2.07 to −2.03 eV) stable binding sites for Se atom on the (11$\bar{2}$0) surface, with only the three most stable ones shown in Figure 5. In particular, Se prefers to coordinate to both surface Cd and surface Se atoms, either between the two neighboring sites or by inserting into a CdSe surface bond at a bridge position. Since Se is only coordinated by one Cd and one Se atom, it is not surprising that it binds more weakly on the (11$\bar{2}$0) surface than on either of the two polar surfaces. On the (11$\bar{2}$0) surface, there are two distinct diffusion pathways, either parallel to the surface CdSe chains in the $\langle 0001\rangle$ direction or perpendicular in the $\langle 10\bar{1}0\rangle$

TABLE 4: Binding Energy of the Cd and Se Atoms and the CdSe Molecule on Various Sites of the Reconstructed CdSe$(0001)_V$ and CdSe$(0001)_A$ Surfaces[a]

BE (eV)	$(0001)_{V,(X\rightarrow V)}$			$(0001)_{A,(X\rightarrow A)}$		
site	Se	Cd[b]	CdSe[c]	Se	Cd[d]	CdSe
top				−0.78		
top_X		−0.33		−3.07		
B2				−2.78		
$B2_X$	$\rightarrow T4_X$			$\rightarrow top_A$		
H3	−0.89			−1.30		
$H3_X$	−0.57					
T4				−1.79		
$T4_X$	−1.42			−2.99	−0.75	
$[top_X-H3_X]$			−2.85			
$[T4_X-top]$						−3.40
$[T4_X-H3]$						$\rightarrow[T4_X-top]$
[T4−H3]						$\rightarrow[T4_X-top]$

[a] Site labels correspond to parts d and e of Figure 3. [b] Same as buckling (0001). [c] Same as Se on H3 site of (0001). [d] Same as CdSe on [T4−B2] site of (0001).

direction. We estimate that the ⟨0001⟩ axis is the easier axis and the $\langle 10\bar{1}0\rangle$ axis is the harder axis for diffusion, with a barrier of at least 0.04 and 0.17 eV over HU and $BL_\perp$ sites, respectively.

The Cd atom, on the other hand, is very weakly bound to the $(11\bar{2}0)$ surface, with several almost degenerate binding sites, with binding energies ranging between −0.30 to −0.25 eV. Like Se atoms, Cd atoms also prefer dual coordination to both Cd and Se surface atoms, but insertion of Cd at the bridge sites of the topmost surface layer is not favored. Again, we estimate the diffusion to be easier along the ⟨0001⟩ axis than along the $\langle 10\bar{1}0\rangle$ axis, with the barrier of at least 0.06 and 0.21 eV over HL and $BU_\perp$ sites, respectively. The weak binding of Cd on the $(11\bar{2}0)$ is similar to that on the polar (0001) surface, with low coordination favored for the bound atom.

The binding energy of the CdSe molecule, −2.66 eV on the $[T1_{Se}-T1_{Cd}]_\perp$ site and −2.59 eV on the $[T1_{Se}-T1_{Cd}]_{||}$ site, is similar to the binding energy of CdSe on the polar Se terminated $(000\bar{1})$ surface, where, in both cases, the molecule is bound primarily through Cd and to a lesser degree through Se. It is also worth pointing out that CdSe prefers to bind in positions that are very similar to the position of the next layer of the bulk truncated structure. In particular, the structure with the adsorbed molecule bridging the surface CdSe chains is slightly preferred relative to the molecule directed parallel to the ⟨0001⟩ direction along the chains. Since we only obtain a few stable binding states for the CdSe molecule, we cannot estimate the diffusion barrier.

2.5. Adsorption on Reconstructed $(0001)_V$ and $(0001)_A$ Surfaces. Schematic representations of high-symmetry binding sites on the vacancy (V) and adatom (A) reconstructions of the (0001) surface are presented in parts d and e of Figure 3. All sites on the reconstructed surfaces are either analogous to the sites on the (0001) surface or adjacent to the vacancy or the adatom site. As a result, we modify the notation for the later ones to include specification V or A to represent a site that is neighboring the vacancy or adatom, respectively. Binding energies of the Cd and Se adatoms and the CdSe molecule at the various sites on the two reconstructed surfaces are presented in Table 4, with the schematics of the most stable binding configurations shown in Figure 6.

On both of the reconstructed surfaces, the preferred binding geometry for the Se atom is in the vicinity of the reconstruction, in particular, the $T4_V$ site (−1.42 eV) and the top_A site (−3.07 eV) on the $(0001)_V$ and the $(0001)_A$ surfaces, respectively. Comparing these binding energies to the binding energy of Se on the (0001) surface reveals that, in the presence of a reconstruction, the binding energy of Se is decreased significantly on the $(0001)_V$ surface and to a lesser extent on the $(0001)_A$ surface. This is not surprising, since the vacancy stabilizes the (0001) surface, making it less reactive. On the other hand, on the $(0001)_A$ surface, the Se atom can interact with the surface adatom, as evidenced by a shift of the Se adatom from the H3 to the B2 site (Figure 6), thus stabilizing adsorption. A similar effect is observed as a result of adsorption of the Cd atom and the CdSe molecule. In particular, the Cd atom binds more strongly on the $(0001)_A$ surface (−0.75 eV) than on either the (0001) or the $(0001)_V$ surface. Binding of the CdSe molecule at the top_V-H3_V site (−2.85 eV) and the $T4_A-$top site (−3.40 eV) on the $(0001)_V$ and $(0001)_A$ surfaces, respectively, is destabilized by a vacancy and enhanced by the adatom. In both cases, the surface adatom shifts from the H3 to the B2 surface site. Since the diffusion of the adatom and the adsorbate would likely occur in unison, the barrier for diffusion cannot be easily estimated.

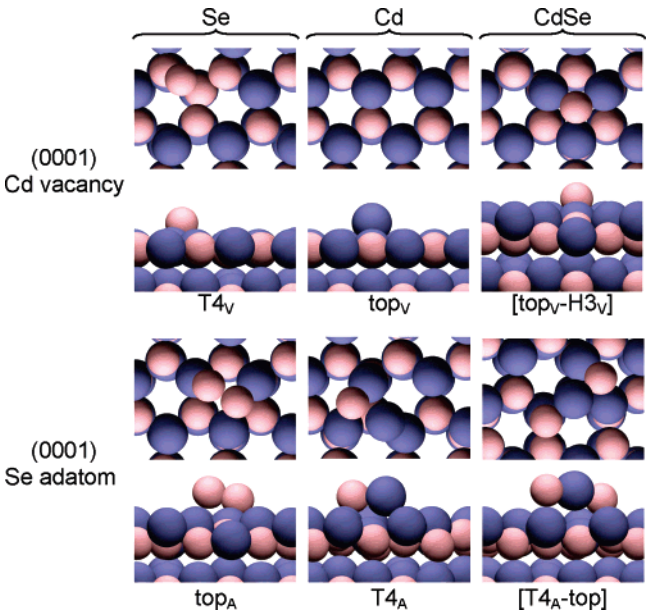

Figure 6. Most stable binding configurations of the Cd and Se atoms and CdSe molecule on the two reconstructed surfaces: $(0001)_V$ and $(0001)_A$.

2.6. Dissociation Thermodynamics. Vibrational frequencies of adsorbates (Se, Cd, and CdSe) in their most stable binding configurations on the three relaxed and two reconstructed surfaces are presented in Table 5, along with the binding energies corrected for the ZPE and the dissociation energies of the adsorbed CdSe molecule. In general, the adsorbates undergo low energy vibrations, and as a result, the ZPE correction is small in comparison to the binding energy, on the order of only a tenth of an eV. A schematic of the thermochemistry of the CdSe binding and dissociation reaction ($CdSe_g \rightarrow CdSe_a \rightarrow Cd_a + Se_a$) on the five surfaces is presented in Figure 7. Comparison of the energetics of the first reaction step shows that CdSe binding is strongest on the relaxed and adatom reconstructed (0001) surface, and in particular, the presence of a Se adatom on the surface enhances subsequent adsorption of the CdSe molecule. Furthermore, comparison of the energetics of the dissociation step shows that on the relaxed and reconstructed (0001) surfaces and on the $(11\bar{2}0)$ surface, dissociation is endothermic, while still preferable to desorption. On the other hand, on the $(000\bar{1})$ surface, dissociation is exothermic, which is attributed to strong binding of the Cd atom on that surface

TABLE 5: Vibrational Frequencies and Binding Energies[a] of the Most Stable Adsorbed Species on the Three Relaxed and Two Reconstructed Surfaces of CdSe. Dissociation Energy[a] of the CdSe Molecule on all Surfaces is also Presented[b]

surface	species	site	frequency[c] (cm^{-1})	BE[BE + ZPE_c] (eV)	ΔE_{dis}[+ZPE_c] (eV)
vacuum	CdSe		192.3		
(0001)	clean, buckle				
	Se	H3	151.9, 104.5, 104.5	−3.59 [−3.57]	
	Cd	top		−0.35 [−0.35]	
	CdSe	[H3−B2]	183.6, 148.9	−3.27 [−3.26]	0.41 [0.42]
(000$\bar{1}$)	Se	B2	186.3, 133.8	−2.90 [−2.88]	
	Cd	H3	105.4, 105.1	−2.09 [−2.08]	
	CdSe	[H3−B2]	246.4, 106.2	−2.63 [−2.62]	−1.29 [−1.27]
(11$\bar{2}$0)	Se	$BL_{\|\|}$	185.4, 161.9	−2.07 [−2.05]	
	Cd	$BL_{\perp}$		−0.30 [−0.30]	
	CdSe	$T1_{Se}$−$T1_{Cd}$	265.0, 147.2, 114.8	−2.66 [−2.64]	1.36 [1.36]
$(0001)_V$	Se	$T4_V$	214.8	−1.42 [−1.41]	
	Cd	top_V		−0.33 [−0.33]	
	CdSe	[top_V−$H3_V$]	170.5, 119.3, 110.1	−2.85 [−2.84]	2.17 [2.17]
$(0001)_A$	clean		151.9, 104.5, 104.5		
	Se	top_A	265.3, 148.6, 125.1	−3.07 [−3.06]	
	Cd	$T4_A$	183.6	−0.75 [−0.75]	
	CdSe	[$T4_A$-top]	274.4, 188.4, 155.2, 144.7	−3.40 [−3.39]	0.65 [0.65]

[a] Binding and dissociation energy corrected for the ZPE shown in the brackets. [b] ΔE_{dis} = 1.07 eV in the gas phase. [c] Only frequencies >100 cm^{-1} are listed.

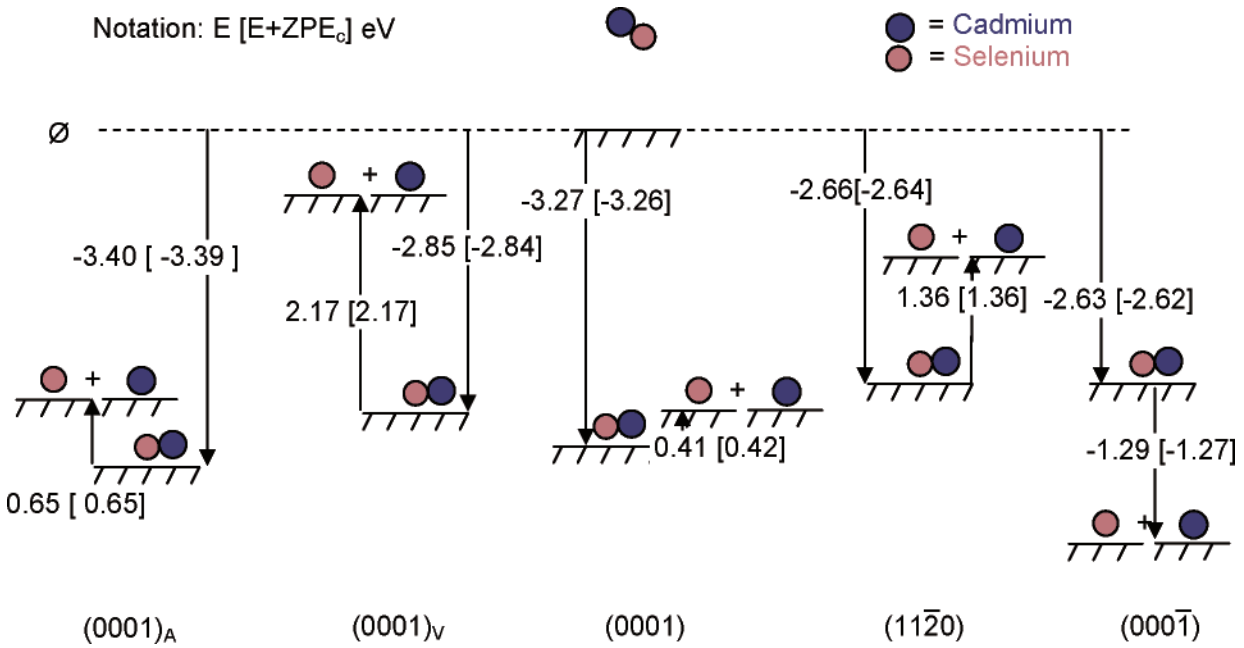

Figure 7. Schematic of the adsorption and dissociation thermodynamics of the CdSe molecule on the three relaxed and two reconstructed surfaces of CdSe. Energies are given relative to the CdSe molecule infinitely separated from the surface.

relative to all the other surfaces. When comparing the adsorption and dissociation reaction thermodynamics in Figure 7, we see that the overall reaction is favored on the (000$\bar{1}$) surface via the formation of Cd_a and Se_a. Furthermore, in analogy to the adatom reconstruction of the (0001) surface, we expect that the presence of the bound Cd and Se atoms will enhance subsequent adsorption on the (000$\bar{1}$) surface, and as a result, we would expect the (000$\bar{1}$) to be, in general, the preferred facet for epitaxial growth.

3. Conclusions

To obtain a better understanding of the crystal growth processes that occur at nanocrystal surfaces, we have performed a comprehensive study of the polar (0001) and (000$\bar{1}$) facets and the nonpolar (11$\bar{2}$0) facet of the wurtzite CdSe using periodic DFT-GGA calculations and, thereon, chemical reactions that are relevant to growth. In particular, we investigated possible mechanisms for surface relaxations and surface reconstructions and related the energies of the two to the ability of the partially filled electronic surface states to become either empty or full via electron transfer. We developed a modified infinite wedge method to determine independently surface energies of the polar facets and compared them to the surface energy of the nonpolar facet. Furthermore, we explored the key elementary reaction steps occurring during crystal growth on the relaxed and the reconstructed surfaces that include adsorption and diffusion of the Cd and Se atoms and adsorption, diffusion, and dissociation of the CdSe molecule. We determined the preferred binding geometries and binding energetics for the atomic and molecular species along with dissociation thermochemistry of the CdSe molecule on the relaxed and reconstructed surfaces. Moreover, we linked all of our findings to the crystal growth of CdSe nanocrystals.

We find that the (11$\bar{2}$0) nanocrystal side surface is overall the most thermodynamically stable surface, while, between the top and bottom polar surfaces, the (000$\bar{1}$) surface is more stable

under Cd poor conditions and the (0001) surface is more stable under Cd rich conditions. This would seem to imply that the two polar surfaces would undergo growth at higher rates. Relaxation significantly stabilizes the (0001) and ($11\bar{2}0$) surfaces and, to a lesser degree, the ($000\bar{1}$) surface, due to a shift in the hybridization of the surface Cd atoms from sp^3 to sp^2 on the former. Reconstructions of the polar surfaces, via either vacancy formation or adatom adsorption, are preferred on the (0001) surface over the ($000\bar{1}$) surface, and as a result, we would expect the (0001) facet to be present in the reconstructed form during nanocrystalline growth.

Binding of the atomic adsorbates is strongest on the (0001) and ($000\bar{1}$) surfaces for the Se and Cd atom, respectively. In both cases, 3-fold coordination of the adsorbates is preferred. On the other hand, binding of the CdSe molecule is favored on the (0001) surface, with the CdSe molecule parallel to the surface. Reconstruction of the (0001) surface upon adsorption of adatoms enhances binding of the Cd atom and the CdSe molecule and only slightly hinders binding of the Se atom. On the other hand, a vacancy on the (0001) surface does not influence Cd atom binding but does hinder binding of the Se atom and the CdSe molecule. Therefore, we would expect growth on the (0001) surface to be enhanced upon adsorption of adatoms and hindered in the presence of vacancies. Dissociation of the CdSe molecule is endothermic on all but the ($000\bar{1}$) surface, while still preferable to desorption. Furthermore, overall binding or binding and dissociation on the relaxed and reconstructed surfaces considered here is thermodynamically favored on the ($000\bar{1}$) surface, which suggests that between the two polar facets, homoepitaxial growth would be favored on the ($000\bar{1}$) Se terminated facet of the nanocrystal.

In summary, the key finding of this work is that, under a reaction-controlled regime, we would expect the rate of homoepitaxy to vary between the side, top, and bottom surfaces of the nanocrystal, with the rate on ($11\bar{2}0$) < (0001) < ($000\bar{1}$) surface. Thus, this makes the Se terminated polar ($000\bar{1}$) surface the primary direction of growth. Moreover, using the formalism developed in this work, we are now able to approach more complicated problems associated with crystal growth of CdSe nanocrystals. For example, we can begin to understand why adding certain ligands to growth solution lead to the formation of quantum dots while others lead to the formation of anisotropic rod structures.

Acknowledgment. Financial support was provided in part by the NSF Materials Research Science and Engineering Center (MRSEC) at the Massachusetts Institute of Technology and by the Hertz Foundation graduate fellowship to J.R. We acknowledge computational resources provided by the National Center for Supercomputing Applications (NCSA), the San Diego Supercomputer Center (SDSC), and the Boston University Scientific Computing Facilities.

References and Notes

(1) Alivisatos, A. P. Perspectives on the physical chemistry of semiconductor nanocrystals. *J. Phys. Chem.* **1996**, *100* (31), 13226−13239.

(2) Murray, C. B.; Kagan, C. R.; Bawendi, M. G. Synthesis and Characterization of Monodisperse Nanocrystals and Close-Packed Nanocrystal Assemblies. *Annu. Rev. Mater. Sci.* **2000**, *30*, 545−610.

(3) Parak, W. J.; Gerion, D.; Pellegrino, T.; Zanchet, D.; Micheel, C.; Williams, S. C.; Boudreau, R.; Gros, M. A. L.; Larabell, C. A.; Alivisatos, A. P. Biological Applications of Colloidal Nanocrystals. *Nanotechnology* **2003**, *14* (7), R15−R27.

(4) Coe, S.; Woo, W. K.; Bawendi, M. G.; Bulovic, V. Electroluminescence from Single Monolayers of Nanocrystals in Molecular Organic Devices. *Nature* **2002**, *420*, 800−803.

(5) Klimov, V. I.; Mikhailovsky, A. A.; Xu, S.; Malko, A.; Hollingsworth, J. A.; Leatherdale, C. A.; Eisler, H. J.; Bawendi, M. G. Optical Gain and Stimulated Emission in Nanocrystal Quantum Dots. *Science* **2000**, *290*, 314−317.

(6) Murray, C. B.; Norris, D. J.; Bawendi, M. G. Synthesis and Characterization of Nearly Monodisperse CdE (E = S, Se, Te) Semiconductor Nanocrystallites. *J. Am. Chem. Soc.* **1993**, *115*, 8706−8715.

(7) Dabbousi, B. O.; Rodriguez-Viejo, J.; Mikulec, F. V.; Heine, J. R.; Mattoussi, H.; Ober, R.; Jensen, K. F.; Bawendi, M. G. (CdSe)ZnS Core-Shell Quantum Dots: Synthesis and Characterization of a Size Series of Highly Luminescent Nanocrystallites. *J. Phys. Chem. B* **1997**, *101*, 9463−9475.

(8) Yen, B. K. H.; Stott, N. E.; Jensen, K. F.; Bawendi, M. G. A Continuous Flow Microcapillary Reactor for the Preparation of High Quality CdSe Nanocrystals. *Adv. Mater.* **2003**, *15* (21), 1858−1862.

(9) Peng, X.; Manna, L.; Yang, W.; Wickham, J.; Scher, E. C.; Kadavanich, A. V.; Alivisatos, A. P., Shape Control of CdSe Nanocrystals. *Nature* **2000**, *404*, 59−61.

(10) Manna, L.; Scher, E. C.; Alivisatos, A. P. Synthesis of Soluble and Processable Rod-, Arrow-, Teardrop-, and Tetrapod- shaped CdSe Nanocrystals. *J. Am. Chem. Soc.* **2000**, *122*, 12700−12706.

(11) Talapin, D. V.; Rogach, A. L.; Haase, M.; Weller, H. Evolution of an Ensemble of Nanoparticles in a Colloidal Solution: Theoretical Study. *J. Phys. Chem.* **2001**, *105*, 12278−12285.

(12) Bullen, C. R.; Mulvaney, P. Nucleation and Growth Kinetics of CdSe Nanocrystals in Octadecene. *Nano Lett.* **2004**, *4* (12), 2303−2307.

(13) Rabani, E. Structure and electrostatic properties of passivated CdSe nanocrystals. *J. Chem. Phys.* **2001**, *115* (3), 1493−1497.

(14) Wang, Y. R.; Duke, C. B. Cleavage faces of wurtzite CdS and CdSe: Surface relaxation and electronic structure. *Phys. Rev. B* **1988**, *37*, 6417−6424.

(15) Manna, L.; Wang, L. W.; Cingolani, R.; Alivisatos, A. P. First-Principles Modeling of Unpassivated and Surfactant-Passivated Bulk Facets of Wurtzite CdSe: A Model System for Studying the Anisotropic Growth of CdSe Nanocrystals. *J. Phys. Chem. B* **2005**, *109* (13), 6183−6192.

(16) Shiang, J. J.; Kadavanich, A. V.; Grubbs, R. K.; Alivisatos, A. P. Symmetry of Annealed Wurtzite CdSe Nanocrystals: Assignment to the C3v Point Group. *J. Phys. Chem.* **1995**, *99*, 17417−17422.

(17) Smith, A. R.; Feenstra, R. M.; Greve, D. W.; Shin, M.-S.; Skowronski, M.; Neugebauer, J.; Northrup, J. E. GaN(0001) surface structures studied using scanning tunneling microscopy and first-principles total energy calculations. *Surf. Sci.* **1999**, *423* (1), 70−84.

(18) Kresse, G.; Dulub, O.; Diebold, U. Competing Stabilization Mechanism for the Polar ZnO(0001)−Zn Surface. *Phys. Rev. B* **2003**, *68* (24), 245409.

(19) Zhang, L.; Tang, H. F., J.; Mavrikakis, M.; Kuech, T. F. The addition of Sb as a surfactant to GaN growth by metal organic vapor phase epitaxy. *J. Appl. Phys.* **2002**, *92* (5), 2304−2309.

(20) Liu, Z. Y.; Gokhale, A. A.; Mavrikakis, M.; Saulys, D. A.; Kuech, T. F. Modifications of the electronic structure of GaSb surface by chalcogen atoms: S, Se, and Te. *J. Appl. Phys.* **2004**, *96* (8), 4302−4307.

(21) Kratzer, P.; Hammer, B.; Nørskov, J. K. The coupling between adsorption dynamics and the surface-structure H2 on Si(100). *Chem. Phys. Lett.* **1994**, *229*, 645.

(22) Hammer, B.; Hansen, L. B.; Nørskov, J. K. Improved adsorption energetics within density-functional theory using revised Perdew-Burke-Ernzerhof functionals. *Phys. Rev. B* **1999**, *59* (11), 7413−7421.

(23) Vanderbilt, D., Soft self-consistent pseudopotentials in a generalized eigenvalue formalism. *Phys. Rev. B* **1990**, *41* (11), 7892−7895.

(24) Perdew, J. P.; Chevary, J. A.; Vosko, S. H.; Jackson, K. A.; Pederson, M. R.; Singh, D. J.; Fiolhais, C. Atoms, molecules, solids, and surfaces: Applications of the generalized gradient approximation for exchange and correlation. *Phys. Rev. B* **1992**, *46* (11), 6671−6687.

(25) White, J. A.; Bird, D. M. Implementation of gradient-corrected exchange-correlation potentials in Car-Parrinello total-energy calculations. *Phys. Rev. B* **1994**, *50* (7), 4954−4957.

(26) Kresse, G.; Furthmuller, J. Efficiency of ab initio total energy calculations for metals and semiconductors using a plane-wave basis set. *Comput. Mater. Sci.* **1996**, *6* (1), 15−50.

(27) Monkhorst, H. J.; Pack, J. D. Special points for Brillouin-zone integrations. *Phys. Rev. B* **1976**, *13* (12), 5188−5192.

(28) *CRC Handbook of Chemistry and Physics*, 76th ed.; CRC Press: New York, 1996

(29) Neugebauer, J.; Scheffler, M. Adsorbate−substrate and adsorbate−adsorbate interactions of Na and K adlayers on Al(111). *Phys. Rev. B* **1992**, *46* (24), 16067−16080.

(30) Zhang, S. B.; Wei, S. H. Surface Energy and the Common Dangling Bond Rule for Semiconductors. *Phys. Rev. Lett.* **2004**, *92* (8), 086102.